Journal of Materials Chemistry C

Accepted Manuscript

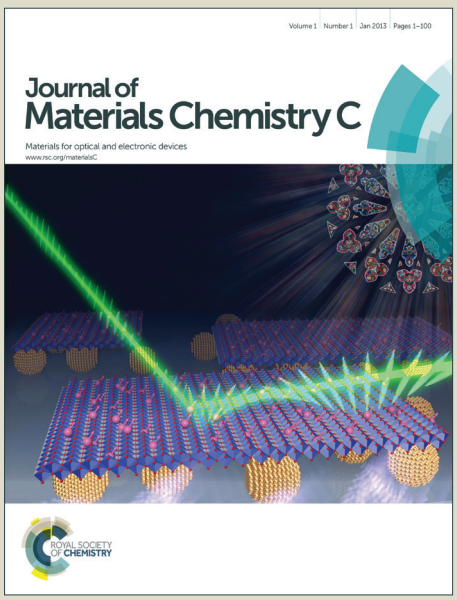

This is an *Accepted Manuscript*, which has been through the Royal Society of Chemistry peer review process and has been accepted for publication.

Accepted Manuscripts are published online shortly after acceptance, before technical editing, formatting and proof reading. Using this free service, authors can make their results available to the community, in citable form, before we publish the edited article. We will replace this *Accepted Manuscript* with the edited and formatted *Advance Article* as soon as it is available.

You can find more information about *Accepted Manuscripts* in the Information for Authors.

Please note that technical editing may introduce minor changes to the text and/or graphics, which may alter content. The journal's standard Terms & Conditions and the Ethical guidelines still apply. In no event shall the Royal Society of Chemistry be held responsible for any errors or omissions in this *Accepted Manuscript* or any consequences arising from the use of any information it contains.

ROYAL SOCIETY OF CHEMISTRY

www.rsc.org/materialsC

Cite this: DOI: 10.1039/c0xx00000x

www.rsc.org/xxxxxx

ARTICLE TYPE

Ambipolar charge-transport property for the D-A complex with naphthalene diimide motif†

Xin Chen, Guanxin Zhang,* Hewei Luo, Yonghai Li, Zitong Liu, Deqing Zhang*

Received (in XXX, XXX) Xth XXXXXXXXX 20XX, Accepted Xth XXXXXXXXX 20XX

DOI: 10.1039/b000000x

A new NDI derivative **4NH$_2$-NDI** was synthesized and investigated. The introduction of four amino groups at core position endows **4NH$_2$-NDI** with a high HOMO energy (-4.87 eV). The OFETs results reveal that **4NH$_2$-NDI** behaves as *p*-type semiconductor with a rather low hole mobility of 8.2×10^{-5} $cm^2\cdot V^{-1}\cdot s^{-1}$. However, its hole mobility can be enhanced significantly after doped with *N*, *N*-dihexyl naphthalene diimide (**DHNDI**). More interestingly, the blend thin films of **4NH$_2$-NDI** and **DHNDI** exhibit ambipolar behavior based on the respective transfer and output characteristics measured in inert atmosphere, and hole and electron mobilities can reach 0.01 $cm^2\cdot V^{-1}\cdot s^{-1}$ and 0.001 $cm^2\cdot V^{-1}\cdot s^{-1}$, respectively, when the molar ratio of **4NH$_2$-NDI** and **DHNDI** is 1:3.

1. Introduction

Organic semiconductors, as active materials for future flexible optoelectronic devices, have received tremendous attentions in recent years.[1] A number of *p*-type organic semiconductors with high hole mobilities have been developed.[2] Remarkable progresses are also achieved for *n*-type organic semiconductors.[3] In comparison, organic ambipolar semiconductors with high and balanced hole/electron mobilities are still limited. However, ambipolar semiconductors are of technological significance for the development of complementary integrated-circuit technology, similar to Si complementary metal-oxide-semiconductor (CMOS) technology.[4] Particularly, organic ambipolar thin film transistors, which integrate both *p*-type and *n*-type channels in one device and thereby simplify circuit design and fabrication process, are attractive for applications in low-cost, flexible, and portable electronic applications.[5]

Normally, pi-conjugated molecules show only unipolar charge transport property. As a consequence, several different approaches have been explored to realize ambipolar organic materials. For example, conjugated molecules and polymers with low band-gaps are promising for ambipolar semiconductor, with the consideration that the low-lying LUMO and high-lying HOMO levels would facilitate the efficient injection and transport of electrons and holes.[6] Along this vein ambipolar semiconductors with mobilities over 1.0 $cm^2\cdot V^{-1}\cdot s^{-1}$ for both charge-carrier species have been described.[7] Some of us reported that the incorporation of both electron donating and accepting moieties to naphthalene diimide (NDI) can effectively tune the HOMO/LUMO levels and the resulting NDI compounds exhibit ambipolar semiconducting properties.[8] Alternatively, electron donor-acceptor (D-A) complexes were investigated for ambipolar charge-transporting properties. Coropceanu, Brédas and their coworkers theoretically predicted the remarkable ambipolar charge-transport properties for mixed-stack D-A complexes.[9] In fact, blend films of either semiconducting polymers/fullerene derivative or *p*-type/*n*-type semiconducting polymers were reported to exhibit ambipolar charge-transporting properties, but their charge mobilities were low and not well balanced.[10] Recently, Zhu, Park and their coworkers have studied the ambipolar charge-transport behavior of crystalline D-A complexes which exhibit relatively high hole and electron mobilities.[11] In this paper we report the ambipolar charge-transport behavior for the thin films of D-A complexes with 2,3,6,7-tetraaminonaphthalene diimide (**4NH$_2$-NDI**) as electron donor and *N, N*-dihexyl naphthalene diimide (**DHNDI**) as electron acceptor.

Naphthalene diimide (NDI) and its derivatives have been intensively investigated for *n*-type semiconductors.[12] It is common to design new *n*-type semiconductors that are stable under OFET device working condition in air by incorporating electron-withdrawing groups into the NDI core to reduce the LUMO energy. For instance, Gao and coworkers synthesized and investigated core-expanded NDI derivatives containing *2*-(*1,3*-dithiol-*2*-ylidene) malonitrile groups (electron-withdrawing) and the resulting organic field effect transistors (OFETs) exhibited electron mobilities of up to 1.2 $cm^2\cdot V^{-1}\cdot s^{-1}$ in air.[13] Also, some of us reported dithiazole-fused NDIs with electron mobilities up to 0.15 $cm^2\cdot V^{-1}\cdot s^{-1}$.[14] In alternative way, incorporation of electron donating groups into the NDI framework can adjust the HOMO/LUMO energies, and the resulting NDIs behave ambipolar and even *p*-type semiconducting properties depending on the electron donating groups.[15]

With this knowledge in mind, it is expected that 2,3,6,7-tetraaminonaphthalene diimide (**4NH$_2$-NDI**, see Scheme 1) may possess high HOMO energy and thus can function as an electron donor. Therefore, **4NH$_2$-NDI** and **DHNDI** are the good electron donor and acceptor, respectively, for the formation of D-A

Journal of Materials Chemistry C Accepted Manuscript

complex which is interesting for investigating the ambipolar charge-transport behavior. In the following, we will firstly report the synthesis and characterization of **4NH$_2$-NDI**, followed by the studies of the OFETs with thin films of the D-A complex of **4NH$_2$-NDI** and **DHNDI**. The results reveal that the D-A complex of **4NH$_2$-NDI** and **DHNDI** exhibits ambipolar semiconducting behavior with hole and electron mobilities of up to 0.01 and 0.001 $cm^2 \cdot V^{-1} \cdot s^{-1}$, respectively.

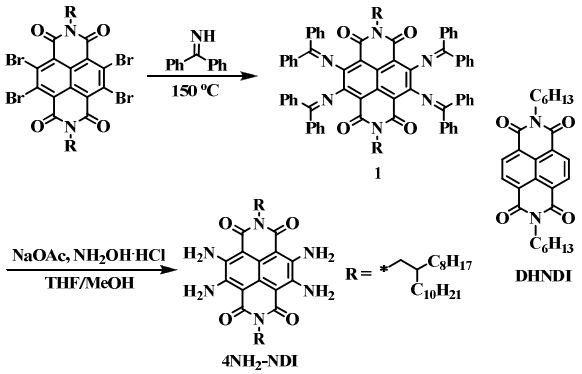

Scheme 1 Synthetic approaches to **4NH$_2$-NDI** and structure of **DHNDI**.

2. Results and discussion

2.1 Synthesis, characterization and HOMO/LUMO energies of 4NH$_2$-NDI

The synthesis of **4NH$_2$-NDI** is shown in Scheme 1. Nucleophilic substitution of 2,3,6,7-tetrabromoNDI (4BrNDI)[16] with benzophenone imine gave the orange compound **1** in 59% yield. Further hydrolysis of **1** under mild conditions afforded compound **4NH$_2$-NDI** in 42% yield. The chemical structure of **4NH$_2$-NDI** was fully characterized with NMR and MS, and its purity was checked with elemental analysis (see Experimental section). **4NH$_2$-NDI** is easily soluble in common organic solvents such as CH_2Cl_2, $CHCl_3$, THF and toluene. Thermogravimetric analysis (TGA) reveals that **4NH$_2$-NDI** is thermally stable below 350 °C (see Fig. S1). Moreover, **4NH$_2$-NDI** is very stable in the solid state and can be kept in air for several months, though four amino units are presented.

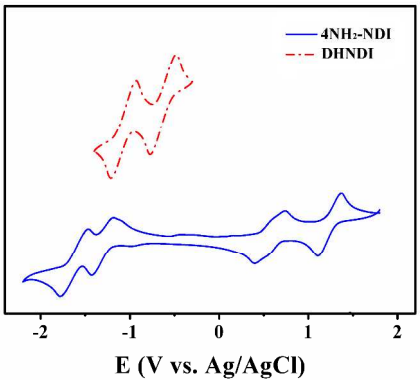

Fig. 1 Cyclic voltammograms of **4NH$_2$-NDI** and **DHNDI** in CH_2Cl_2 (1.0×10^{-3} M) at a scan rate of 100 $mV \cdot s^{-1}$, with glassy carbon electrode as the working electrode, Pt as the counter electrode and Ag/AgCl electrode (saturated KCl) as the reference electrode, and *n*-Bu_4NPF_6 (0.1 M) as supporting electrolyte.

As shown in Fig. 1, **4NH$_2$-NDI** exhibits two reversible oxidation waves with $E^{1/2}(ox_1)$ = 0.57 V and $E^{1/2}(ox_2)$ = 1.24 V, and two reversible reduction waves with $E^{1/2}(red_1)$ = -1.31 V and $E^{1/2}(red_2)$ = -1.62 V. Accordingly, LUMO and HOMO energies [LUMO = -(E_{onset}^{red1} + 4.41) eV, HOMO = -(E_{onset}^{ox1} + 4.41) eV][17] of **4NH$_2$-NDI** were estimated to be -3.18 eV and -4.87 eV on the basis of the respective onset reduction and oxidation potentials, respectively. Such a high HOMO energy (-4.87 eV) indicates that **4NH$_2$-NDI** is transformed into an electron donor because of the incorporation of four amino groups in the NDI motif.

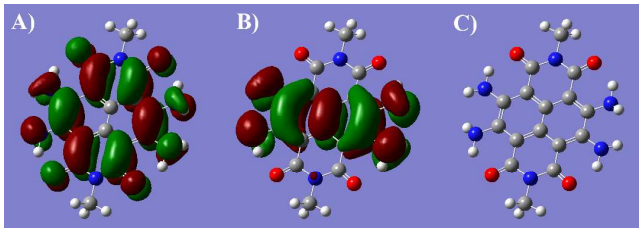

Fig. 2 LUMO (A), HOMO (B) orbital and structure (C) of **4NH$_2$-NDI** obtained by DFT calculations; the alkyl chains were replaced by methyl groups in the calculations.

The chemical structure of **4NH$_2$-NDI** was investigated with theoretical calculations based on density functional theory (DFT). It is expected that the alkyl chains at the *N, N'*-positions of NDI cores in **4NH$_2$-NDI** should not have strong influences on its electronic structures. Thus, the alkyl chains were replaced by methyl groups for the DFT calculations. As depicted in Fig. 2, HOMO orbitals of **4NH$_2$-NDI** reside mainly on the naphthalene ring and the four amino groups. In comparison, LUMO orbitals of **4NH$_2$-NDI** are distributed throughout the whole NDI core, and four amino groups also make contribution to the LUMO orbital. One of the hydrogen atoms on each amino group is coplanar with the NDI core, and forms a hydrogen bond with the oxygen atom of the carbonyl group. The calculated LUMO and HOMO energies were -2.50 eV and -5.16 eV, respectively, which are different from those based on redox potentials of **4NH$_2$-NDI**. But, it is understandable as solvent effects were not included in the calculations.

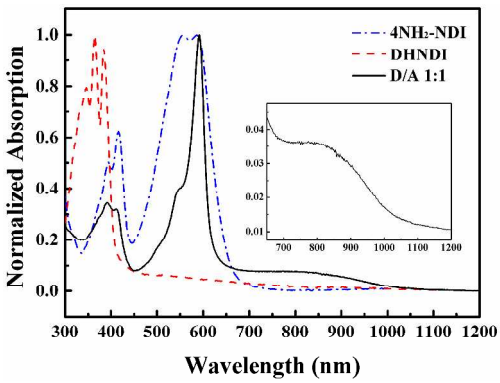

Fig. 3 The absorption spectra of thin films of **4NH$_2$-NDI**, **DHNDI** and their 1:1 mixture.

Fig. 3 shows the absorption spectra of thin films of **DHNDI** and **4NH$_2$-NDI** as well as that of the thin film of the 1:1 mixture of **DHNDI** and **4NH$_2$-NDI**. Thin film of **DHNDI** absorbs strongly around 360 nm, whereas thin film of **4NH$_2$-NDI** shows absorptions around 400 nm and 570 nm. The strong absorption

This journal is © The Royal Society of Chemistry [year]

Journal of Materials Chemistry C Accepted Manuscript

around 570 nm for thin film of **4NH$_2$-NDI** may be interpreted as intramolecular charge-transfer absorption within **4NH$_2$-NDI**. Apart from the absorptions around 400 nm and 590 nm, thin film of the 1:1 mixture of **DHNDI** and **4NH$_2$-NDI** shows absorption tail in the range of 700-1100 nm. The absorption spectra of blend thin films of **DHNDI** and **4NH$_2$-NDI** in other molar ratios were also measured, and such long absorption tail was also observed (Fig. S2). This broad weak absorption is probably owing to the intermolecular D-A interaction among molecules of **4NH$_2$-NDI** and **DHNDI**.

2.2 Fabrication of OFETs and characterization of semiconducting properties

Bottom gate bottom contact OFETs with thin films of **4NH$_2$-NDI** and blends of **4NH$_2$-NDI** and **DHNDI** with different molar ratios were fabricated by spin-coating of the respective solutions onto the substrates (*n*-octadecyltrichlorosilane (OTS) modified SiO_2 surface). The OFET devices were examined both in air and N_2 atmosphere and the corresponding transfer and output characteristics were measured. Based on the transfer characteristics shown in Fig. S3, thin film of **4NH$_2$-NDI** behaves as *p*-type semiconductor with relatively low hole mobility of 8.2×10^{-5} $cm^2\cdot V^{-1}\cdot s^{-1}$ even after thermal annealing at 80 °C (see Table 1). Note that *n*-type semiconducting property was not observed for thin film of **4NH$_2$-NDI** even under nitrogen atmosphere. This is in agreement with the high LUMO energy of **4NH$_2$-NDI** (-3.18 eV).

Table 1 The mobilities (μ), threshold voltages (V_{th}), and on/off ratios ($I_{on/off}$) for bottom contact OFET devices based on thin films of **4NH$_2$-NDI** and blend systems after annealing at different temperatures measured in air.[a]

Compd.	Temp. /°C	μ_h/cm^2·V^{-1}·s^{-1} [b]	$I_{on/off}$	V_{th}/V
4NH$_2$-NDI	**25**	1.1×10^{-5}/6.5×10^{-6}	10^3~10^4	-18~-25
	80	8.2×10^{-5}/4.8×10^{-5}	10^3~10^4	-12~-18
	120	5.0×10^{-5}/2.7×10^{-5}	10^4~10^5	-15~-20
D/A 2:1	**25**	8.7×10^{-4}/5.8×10^{-4}	10^6~10^7	-20~-29
	80	4.6×10^{-3}/1.5×10^{-3}	10^6~10^7	-14~-18
	120	7.6×10^{-4}/4.7×10^{-4}	10^4~10^5	-15~-22
D/A 1:1	**25**	1.0×10^{-3}/5.7×10^{-4}	10^5~10^6	-23~-35
	80	5.6×10^{-3}/3.2×10^{-3}	10^5~10^6	-22~-30
	120	3.3×10^{-3}/1.7×10^{-3}	10^5~10^6	-18~-26
D/A 1:2	**25**	1.8×10^{-3}/7.8×10^{-4}	10^4~10^5	-17~-28
	80	8.8×10^{-3}/5.6×10^{-3}	10^4~10^5	-19~-25
	120	5.5×10^{-3}/3.4×10^{-3}	10^5~10^6	-15~-23
D/A 1:3	**25**	2.6×10^{-3}/9.7×10^{-4}	10^4~10^5	-18~-27
	80	1.8×10^{-2}/1.4×10^{-2}	10^4~10^5	-14~-22
	120	1.4×10^{-2}/1.0×10^{-2}	10^4~10^5	-15~-24
D/A 1:4	**25**	2.2×10^{-3}/8.6×10^{-4}	10^4~10^5	-16~-27
	80	1.4×10^{-2}/8.7×10^{-3}	10^4~10^5	-14~-23
	120	7.7×10^{-3}/5.2×10^{-3}	10^3~10^4	-23~-28

[a] The performance data were obtained based on more than 10 OFET devices. [b] $\mu_{high}/\mu_{average}$

Interestingly, hole mobility of thin film of **4NH$_2$-NDI** can be significantly enhanced after doped with **DHNDI**. OFETs with blend thin films of **4NH$_2$-NDI** and **DHNDI** of different molar ratios were investigated. The results reveal that i) hole mobilities of the blend thin films are affected by the molar ratios of **4NH$_2$-NDI** and **DHNDI**; ii) hole mobilities of the blend thin films are improved after thermal annealing. As listed in Table 1, the thin film with molar ratio of 1:3 (**4NH$_2$-NDI**:**DHNDI**) exhibited the highest hole mobility. The maximum hole mobility (0.018 $cm^2\cdot V^{-1}\cdot s^{-1}$) was achieved for this thin film after thermal annealing at 80 °C. Note that the hole mobility of the blend thin film of **4NH$_2$-NDI** and **DHNDI** (1:3 in molar ratio) is two orders higher than that of the thin film composed of only **4NH$_2$-NDI** under the same conditions. As to be discussed below, the hole mobility enhancement for thin film of **4NH$_2$-NDI** after doped with **DHNDI** may be attributed to the fact that the presence of **DHNDI** increases the molecular order degree in the blend thin film based on XRD data (see Fig. 5).[18]

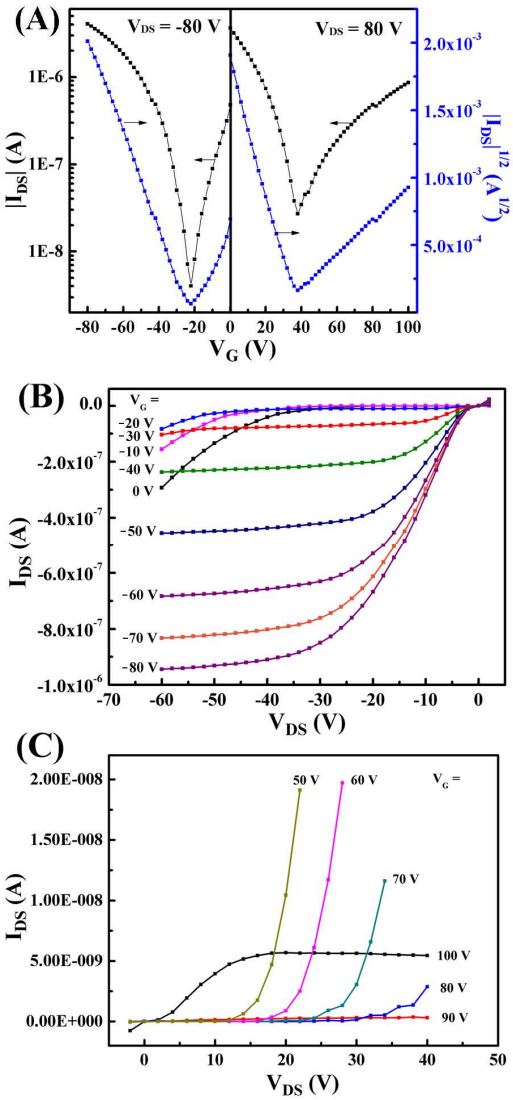

Fig. 4 Transfer and output characteristics for OFETs of mixture of **4NH$_2$-NDI** and **DHNDI** (with the D/A molar ratio of 1:3) measured in N_2; the channel width (W) and length (L) were 1440 μm and 50 μm, respectively.

Journal of Materials Chemistry C Accepted Manuscript

N-type charge transport property was not detected for blend thin films of **4NH$_2$-NDI** and **DHNDI** in air. This is understandable by considering the relatively high LUMO energy of **DHNDI**. Interestingly, blend thin films of **4NH$_2$-NDI** and **DHNDI** do show ambipolar charge transport behavior. As an example, Fig. 4 depicts the OFET transfer and output characteristics, which were measured under N_2, with a blend thin film of **4NH$_2$-NDI** and **DHNDI** (1:3 in molar ratio) after annealing at 80 ^oC. Obviously, V-shape transfer curves, being typical for ambipolar semiconducting behavior, were observed. As listed in Table 2, hole and electron mobilities of as-prepared OFETs were deduced to be 1.6×10^{-3} $cm^2\cdot V^{-1}\cdot s^{-1}$ and 9.6×10^{-4} $cm^2\cdot V^{-1}\cdot s^{-1}$, respectively, based on the respective transfer curves. As expected, the hole mobility was enhanced after thermal annealing, reaching 0.010 $cm^2\cdot V^{-1}\cdot s^{-1}$ (being close to that measured in air) after thermal annealing at 80 ^oC (see Table 2) But, further thermal annealing led to the decrease of hole mobility. In comparison, the electron mobility of the blend thin film didn't vary remarkably upon thermal annealing. In fact, electron mobility of this blend thin film is almost the same as that of **DHNDI** thin film under the same conditions. Semiconducting behaviors of blend thin films of **4NH$_2$-NDI** and **DHNDI** with other molar ratios were also investigated. The results reveal that the blend thin film of **4NH$_2$-NDI** and **DHNDI** (1:3 in molar ratio) shows the best ambipolar semiconducting performance. By considering the respective HOMO/LUMO energies of **4NH$_2$-NDI** and **DHNDI**, the hole and electron transporting properties of the blend thin film should be attributed to **4NH$_2$-NDI** and **DHNDI**, respectively.

Table 2 The mobilities (μ), threshold voltages (V_{th}), and on/off ratios ($I_{on/off}$) for bottom contact OFET devices after annealing at different temperatures measured in N_2 atmosphere. [a]

Condition	Compd.	Temp./^{o}C	μ_h/$cm^2\cdot V^{-1}\cdot s^{-1}$ [b]	$I_{on/off}$	V_{th}/V	μ_e/$cm^2\ V^{-1}\ s^{-1}$ [b]	$I_{on/off}$	V_{th}/V
N_2	4NH$_2$-NDI	25	8.8×10^{-6}/5.7×10^{-6}	10^3~10^4	-20~-30	—	—	—
		80	5.7×10^{-5}/2.3×10^{-5}	10^3~10^4	-15~-29	—	—	—
		120	3.6×10^{-5}/2.4×10^{-5}	10^3~10^4	-16~-31	—	—	—
	DHNDI	25	—	—	—	8.6×10^{-4}/6.5×10^{-4}	10^5~10^6	62~75
		80	—	—	—	1.0×10^{-3}/8.5×10^{-4}	10^5~10^6	60~70
		120	—	—	—	1.0×10^{-4}~6.2×10^{-5}	10^5~10^6	65~78
	2:1	25	6.5×10^{-4}/4.8×10^{-4}	10^2~10^3	-22~-35	8.3×10^{-4}/6.8×10^{-4}	50~100	35~46
		80	2.8×10^{-3}/1.6×10^{-3}	10^2~10^3	-19~-24	7.9×10^{-4}/5.1×10^{-4}	50~100	30~43
		120	9.1×10^{-4}/6.8×10^{-4}	10^2~10^3	-25~-35	3.8×10^{-4}~2.1×10^{-4}	50~100	28~37
	1:1	25	8.6×10^{-4}/5.8×10^{-4}	10^3~10^4	-20~-29	8.2×10^{-4}/6.4×10^{-4}	50~100	35~45
		80	7.3×10^{-3}/3.9×10^{-3}	10^3~10^4	-25~-32	9.2×10^{-4}/7.6×10^{-4}	50~100	25~40
		120	4.3×10^{-3}/2.4×10^{-3}	10^3~10^4	-26~-40	4.3×10^{-4}/2.2×10^{-4}	50~100	26~38
	1:2	25	1.0×10^{-3}/6.2×10^{-4}	10^3~10^4	-18~-32	8.5×10^{-4}/6.8×10^{-4}	50~100	31~38
		80	8.2×10^{-3}/5.6×10^{-3}	10^3~10^4	-20~-27	9.7×10^{-4}/7.6×10^{-4}	50~100	25~38
		120	5.9×10^{-3}/4.1×10^{-3}	10^3~10^4	-27~-32	3.0×10^{-4}/1.7×10^{-4}	50~100	29~42
	1:3	25	1.6×10^{-3}/8.1×10^{-4}	10^3~10^4	-18~-27	9.6×10^{-4}/7.3×10^{-4}	50~100	30~38
		80	1.0×10^{-2}/8.4×10^{-3}	10^3~10^4	-25~-27	1.1×10^{-3}/8.2×10^{-4}	50~100	28~36
		120	8.8×10^{-3}/6.8×10^{-3}	10^3~10^4	-25~-28	6.5×10^{-4}/4.8×10^{-4}	50~100	28~38
	1:4	25	1.1×10^{-3}/6.0×10^{-4}	10^3~10^4	-19~-26	8.3×10^{-4}/6.6×10^{-4}	50~100	30~42
		80	8.1×10^{-3}/6.8×10^{-3}	10^3~10^4	-20~-28	8.9×10^{-4}/6.5×10^{-4}	50~100	25~38
		120	6.1×10^{-3}/4.2×10^{-3}	10^3~10^4	-28~-32	3.6×10^{-4}/1.1×10^{-4}	50~100	28~40

[a] The performance data were obtained based on more than 10 OFET devices. [b] $\mu_{high}/\mu_{average}$

2.3 XRD and AFM studies

XRD and AFM studies were performed for thin films of **4NH$_2$-NDI**, **DHNDI** and the blend thin films in order to understand the variation of charge mobilities after formation of blend thin films and thermal annealing. As depicted in Fig. 5(A) the as-prepared thin film of **4NH$_2$-NDI** shows two weak diffraction peaks at 5.4^o and 8.2^o, which become weak after thermal annealing at 80 ^oC; but further annealing at 120 ^oC leads to slight enhancement for these two XRD signals. In comparison, the as-prepared thin film of **DHNDI** shows a strong diffraction peak at 6.3^o, and multiple weak diffraction peaks at 4.9^o, 12.5^o, 18.7^o, 25.0^o. The diffraction peak at 6.3 ^{o} corresponds to a *d*-spacing of 1.39 nm, and those at 12.5^o, 18.7^o, 25.0^o may be owing to the corresponding second-, third- and fourth-order diffractions. It is obvious that thin film of **DHNDI** shows better crystallinity than thin film of **4NH$_2$-NDI**. After thermal annealing at 80 ^oC the weak XRD signal at 4.9^o disappears, and simultaneously the intensity of the signal at 6.3^o

This journal is © The Royal Society of Chemistry [year]

Journal of Materials Chemistry C Accepted Manuscript

increases.

Fig. 5(C) shows XRD profile for the blend thin film of **4NH$_2$-NDI** and **DHNDI** (1:3 in molar ratio). Interestingly, the blend thin film shows multiple diffraction peaks at 3.5°, 4.9°, 6.3°, 7.0°, 10.5°, and 25.0°, indicating that such blend thin films possesses good crystallinity. After close examination of XRD data, the diffraction signals at 4.9°, 6.3°, 25.0° corresponds well to those of **DHNDI** thin film. The diffraction peaks at 3.5°, 7.0° and 10.5° may be due to **4NH$_2$-NDI** film with a *d*-spacing of 2.49 nm. The signals at 7.0° and 10.5° are due to the corresponding second- and third-order diffractions. After thermal annealing at 80 °C the intensity of the signal at 3.5° increases remarkably, and simultaneously new diffraction peaks at 12.5°, 18.7° appear. Further annealing leads to the decrease for signal at 3.5° and that at 6.3° increases. It may be inferred from these XRD data that the crystallinity of the blend thin film is further improved after thermal annealing. Thus, **DHNDI** molecules may function as crystalline nucleuses to induce the intermolecular order-packing of **4NH$_2$-NDI** molecules. These XRD data agree well with the observation that the blend thin film of **4NH$_2$-NDI** and **DHNDI** exhibit relatively high hole and electron mobilities after thermal annealing.

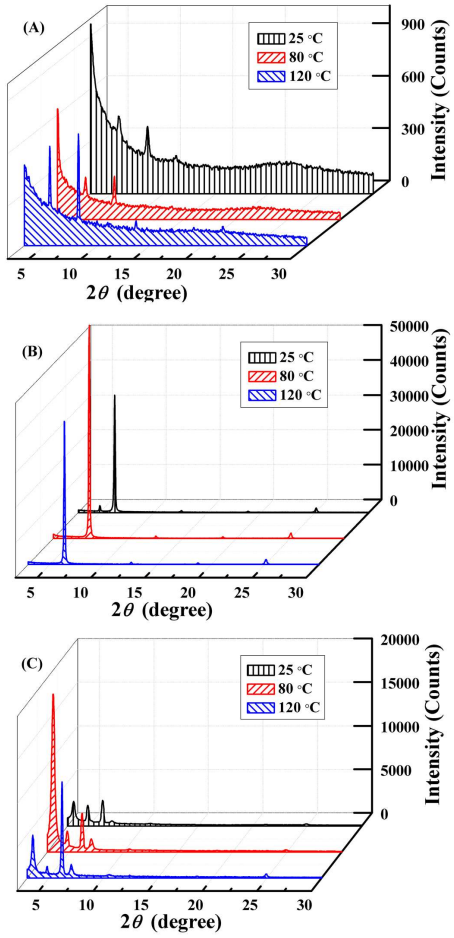

Fig. 5 XRD patterns of thin films of **4NH$_2$-NDI** (A), **DHNDI** (B), and their mixture with D/A molar ratio 1:3 (C) after different annealing temperatures.

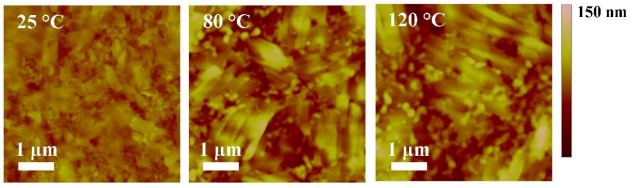

Fig. 6 AFM images of the blend thin film of **4NH$_2$-NDI** and **DHNDI** (1:3 in molar ratio) after annealing at different temperatures.

AFM images of the blend thin film of **4NH$_2$-NDI** and **DHNDI** (1:3 in molar ratio) were depicted in Fig. 6. Plate-like microstructures were formed after thermal annealing at 80 °C. The formation of plate-like microstructures agrees with the improvement of thin film crystallinity, and thus such thin film morphology may be beneficial for charge transport. However, more boundary areas emerged after further annealing at 120°. For comparison, AFM images of thin films of **4NH$_2$-NDI** and **DHNDI** were also given (see Figure S5).

3. Conclusion

In summary, a tetraamino core-substituted NDI derivative **4NH$_2$-NDI** was synthesized and studied. Unlike most of the NDI derivatives, **4NH$_2$-NDI** possesses a high HOMO energy (-4.87 eV) and can function as an electron donor. Thin film of **4NH$_2$-NDI** behaves as *p*-type semiconductor in air condition, but with a rather low hole mobility of 8.2×10^{-5} $cm^2\cdot V^{-1}\cdot s^{-1}$. However, its hole mobility can be improved significantly after being doped by using the parent NDI (**DHNDI**) as an electron acceptor. More interestingly, The blend thin films of **4NH$_2$-NDI** and **DHNDI** display ambipolar behavior based on the respective transfer and output characteristics measured under inert atmosphere. The hole and electron mobilities can reach 0.01 $cm^2\cdot V^{-1}\cdot s^{-1}$ and 0.001 $cm^2\cdot V^{-1}\cdot s^{-1}$, respectively, when the molar ratio of **4NH$_2$-NDI** and **DHNDI** is 1:3. The results demonstrate an efficient way to prepare ambipolar thin-film semicondcutors with NDI derivatives. Further studies will focus on D-A complexes of **4NH$_2$-NDI** with other NDI based electron acceptors to develop air-stable ambipolar semiconducting materials.

4. Experimental section

4.1 Materials

All chemicals were purchased from Alfa Aesar and Sigma-Aldrich, and used as received. All solvents were purified and dried following standard procedures unless otherwise stated. **DHNDI** were prepared according to previous report.[19]

Synthesis of compound 1. A mixture of 4BrNDI (228 mg, 0.20 mmol) and benzophenone imine (0.5 mL) was heated at 150 °C for 10 h under nitrogen. After cooling to room temperature, the mixture was recrystallized from CH_2Cl_2 and EtOH. After filtration, the residue was subjected to column chromatography with petroleum ether (60-90 °C)/CH_2Cl_2 (1:1, v/v) as eluent to give **1** as an orange solid (182 mg) in 59% yield. M.p. 128.7-129.4 °C . ^{1}H NMR (400 MHz, CD_2Cl_2) δ 7.48 (d, 16H), 7.36 (t, 8H), 7.27 (t, 16H), 3.82 (d, 4H), 1.85-1.70 (m, 2H), 1.35-1.07 (m, 64H), 0.92-0.80 (m, 12H). ^{13}C NMR (100 MHz, $CDCl_3$) δ 167.35, 162.87, 146.27, 138.26, 130.11, 129.14, 128.13, 121.65, 110.03, 44.35, 36.34, 32.30, 31.75, 30.57, 30.11, 30.05, 29.73,

Journal of Materials Chemistry C Accepted Manuscript

29.70, 26.76, 23.06, 23.03, 14.49. MALDI-TOF: 1543.3 (M^+). Elemental analysis: calcd. for $C_{106}H_{122}N_6O_4$: C, 82.45; H, 7.96; N, 5.44; found: C, 82.55; H, 7.88; N, 5.30.

Synthesis of 4NH$_2$-NDI. To a mixture of compound **1** (300 mg, 0.20 mmol) and sodium acetate (790 mg, 9.6 mmol) in 100 mL THF/MeOH (1:1, v/v) was added hydroxylamine hydrochloride (500 mg, 7.2 mmol). The mixture was refluxed for 24h under nitrogen. After cooling to room temperature, the mixture was diluted with water and extracted with CH_2Cl_2. The organic layer was dried with Na_2SO_4 and filtrated. After removal of the solvents under vacuum, the residue was subjected to column chromatography with petroleum ether (60-90 ^oC)/CH_2Cl_2 (1:2, v/v) as eluent to give 4NH$_2$-NDI as a purple solid (74 mg) in 42% yield. M.p. 142.5-143.3 ^oC. ^1H NMR (400 MHz, CD_2Cl_2) δ 6.77 (br, 8H), 4.00 (d, 4H), 1.98-1.80 (m, 2H), 1.48-1.07 (m, 64H), 0.95-0.72 (m, 12H). ^{13}C NMR (100 MHz, CD_2Cl_2) δ 166.66, 141.80, 114.85, 103.34, 44.45, 37.07, 32.52, 32.32, 30.71, 30.27, 29.96, 27.11, 23.27, 14.47. MALDI-TOF: 887.1 (M^+); Elemental analysis: calcd. for $C_{54}H_{90}N_6O_4$: C, 73.09; H, 10.22; N, 9.47; found: C, 73.18; H, 10.27; N, 9.43.

4.2 General measurement and characterization

Melting points were measured with Büchi B540. ^1H NMR and ^{13}C NMR spectra were recorded on Bruker AVANCE III 400 MHz spectrometer. MALDI-TOF MS spectra were recorded with BEFLEX III spectrometer. Elemental analysis was performed on a Carlo Erba model 1160 elemental analyzer. TGA (SHIMADZU DTG-60) measurements were performed under nitrogen atmosphere at a heating rate of 10 °C/min. Thin films absorption spectra were measured with JASCO V-570 UV-Vis spectrophotometer. Cyclic voltammetric measurements were carried out in a standard three-electrode cell using a glassy carbon working electrode, a Pt counter electrode and a Ag/AgCl (saturated KCl) reference electrode on a computer-controlled CHI660C instrument. The scan rate was 100 $mV{\cdot}s^{-1}$, and *n*-Bu_4NPF_6 (0.1 M) was used as the supporting electrolyte.

X-ray diffraction (XRD) measurements were carried out in the reflection mode at room temperature, using a 2-kW Rigaku X-ray diffraction system. The thin film surfaces were examined by tapping-mode AFM using Digital Instruments Nanoscope V atomic force microscope in ambient air condition. AFM samples and microscopic images were identical to those used in organic filed-effect transistors. The molecular structures of the compounds were calculated with the DFT method at B3LYP/6-31G (d, p) level. All calculations were performed with the Gaussian 09 program.

4.3 Fabrication and characterization of OFET devices

Bottom gate bottom contact OFETs were fabricated with conventional techniques. Briefly, a heavily doped *n*-type Si wafer and a layer of dry oxidized SiO_2 (300 nm, with roughness lower than 0.1 nm and capacitance of 11 $nF{\cdot}cm^{-2}$) were used as a gate electrode and gate dielectric layer, respectively. The drain-source (*D*-*S*) gold contacts were fabricated by photo-lithography. The channel length and width are 50 μm and 1440 μm, respectively. The substrates were cleaned in water, deionized water, alcohol, and rinsed in acetone. Then, the surface was modified with *n*-octadecyltrichlorosilane (OTS). **4NH$_2$-NDI**, **DHNDI**, and their mixtures with different ratios were dissolved in $CHCl_3$ (about 15 mg/mL) and spin-coated on the above substrate at 2000 rpm. The annealing processes were carried in vacuum condition for 1.0 hr at each temperature.

Field-effect characteristics of the devices were determined in air and nitrogen by using a Keithley 4200 SCS semiconductor parameter analyzer. Carrier mobilities were calculated by fitting a straight line to the plot of the square root of I_{DS} vs. V_G (saturation region), according to the expression $I_{DS}=(W/2L)\mu_e C_i(V_G-V_{TH})^2$.

Notes and references

†*CAS Key Laboratory of Organic Solids, Institute of Chemistry, Chinese Academy of Sciences, Beijing 100190, China. E-mail: dqzhang@iccas.ac.cn*

Electronic Supplementary Information (ESI) available: TGA analysis, UV-Vis spectra, DFT calculation data, OFET performances, AFM images, ^1H NMR and ^{13}C NMR spectra of all new compounds. See DOI: 10.1039/b000000x/.

1 (a) H. Klauk, Organic Electronics: Materials, Manufacturing and Applications; Wiley-VCH: Weinheim: Germany, 2006; (b) A. Murphy and J. Fréchet, *Chem. Rev.*, 2007, **107**, 1066; (c) J. Anthony, A. Facchetti, M. Heeney, S. Marder, X. Zhan, *Adv. Mater.*, 2010, **22**, 3876; (d) A. Virkar, S. Mannsfeld, Z. Bao and N. Stingelin, *Adv. Mater.*, 2010, **22**, 3857; (e) P. Beaujuge, J. Fréchet, *J. Am. Chem. Soc.*, 2011, **133**, 20009; (f) J. Mei, Y. Diao, A. Appleton, L. Fang, Z. Bao, *J. Am. Chem. Soc.*, 2013, **135**, 6724; (g) C. B. Nielsen, M. Turbiez, I. McCulloch, *Adv. Mater.*, 2013, **25**, 1859; (h) R. Pfattner, E. Pavlica, M. Jaggi, S. Liu, S. Decurtins, G. Bratina, J. Veciana, M. Mas-Torrent and C. Rovira, *J. Mater. Chem. C*, 2013, **1**, 3985; (i) E. Glowacki, G. Voss, N. Sariciftci, *Adv. Mater.*, **25**, 6783.

2 (a) W. Jiang, Y. Li, Z. Wang, *Chem. Soc. Rev.*, 2013, **42**, 6113; (b) W. Liu, Y. Zhou, Y. Ma, Y. Cao, J. Wang and J. Pei, *Org. Lett.*, 2007, **9**, 4187; (b) I. Osaka, T. Abe, S. Shinamura, E. Miyazaki and K. Takimiya, *J. Am. Chem. Soc.*, 2010, **132**, 5000; (c) Q. Shen, Y. Cao, S. Liu, L. Gan, J. Li, Z. Wang, J. Hui, X. Guo, D. Xu and Z. Liu, *J. Phys. Chem. Lett.*, 2010, **1**, 1269; (d) I. Osaka, T. Abe, S. Shinamura, K. Takimiya, *J. Am. Chem. Soc.*, 2011, **133**, 6852; (e) T. Lei, Y. Cao, Y. Fan, C. Liu, S. Yuan and J. Pei, *J. Am. Chem. Soc.*, 2011, **133**, 6099; (f) H. Zhang, X. Guo, J. Hui, S. Hu, W. Xu and D. Zhu, *Nano Lett.*, 2011, **11**, 4939; (g) K. Takimiya, S. Shinamura, I. Osaka and E. Miyazaki, *Adv. Mater.*, 2011, **23**, 4347; (h) K. Kuribara, H. Wang, N. Uchiyama, K. Fukuda, T. Yokota, U. Zschieschang, C. Jaye, D. Fischer, H. Klauk, T. Yamamoto, K. Takimiya, M. Ikeda, H. Kuwabara, T. Sekitani, Y. Loo and T. Someya, *Nat. Commun.*, 2012, **3**:723.

3 (a) H. Katz, A. Lovinger, J. Johnson, C. Kloc, T. Siegrist, W. Li, Y. Lin and A. Dodabalapur, *Nature*, 2000, **404**, 478; (b) F. Würthner, *Angew. Chem., Int. Ed.*, 2001, **40**, 1037; (c) B. Jones, A. Facchetti, M. Wasielewski and T. Marks, *J. Am. Chem. Soc.*, 2007, **129**, 15259; (d) R. Schmidt, J. Oh, Y. Sun, M. Deppisch, A. Krause, K. Radacki, H. Braunschweig, M. Könemann, P. Erk, Z. Bao and F. Würthner, *J. Am. Chem. Soc.*, 2009, **131**, 6215; (e) A. Lv, Y. Li, W. Yue, L. Jiang, H. Dong, G. Zhao, Q. Meng, W. Jiang, Y. He, Z. Li, Z. Wang and W. Hu, *Chem. Comm.*, 2012, **48**, 5154; (f) W. Yue, A. Lv, J. Gao, W. Jiang, L. Hao, C. Li, Y. Li, L. Polander, S. Barlow, W. Hu, S. Di Motta, F. Negri, S. Marder and Z. Wang, *J. Am. Chem. Soc.*, 2012, **134**, 5770.

4 (a) M. Shkunov, R. Simms, M. Heeney, S. Tierney, I. McCulloch, *Adv. Mater.*, 2005, **17**, 2608; (b) H. Usta, A. Facchetti, T. J. Marks, *J. Am. Chem. Soc.*, 2008, **130** , 8580; (c) R. Capelli, S. Tofanin, G. Generali, H. Usta, A. Facchetti, M. Muccini, *Nat. Mater.*, 2010, **9**, 496.

5 (a) J. Zaumseil and H. Sirringhaus, *Chem. Rev.*, 2007, **107**, 1296; (b) C. Wang, H. Dong, W. Hu, Y. Liu, D. Zhu, *Chem. Rev.*, 2012, **112**, 2208; (c) Y. Zhao, Y. Guo and Y. Liu, *Adv. Mater.*, 2013, **25**, 5372; (d) S. Bisri, C. Piliego, J. Gao, and M. Loi, *Adv. Mater.*, 2013, DOI: 10.1002/adma.201304280.

Journal of Materials Chemistry C Accepted Manuscript

This journal is © The Royal Society of Chemistry [year]

6 (a) J. Bijleveld, A. Zoombelt, S. Mathijssen, M. Wienk, M. Turbiez, D. de Leeuw, R. Janssen, *J. Am. Chem. Soc.*, 2009, **131**, 16616; (b) H. Bronstein, Z. Chen, R. Ashraf, W. Zhang, J. Du, J. Durrant, P. Tuladhar, K. Song, S. Watkins, Y. Geerts, M. Wienk, R. Janssen, T. Anthopoulos, H. Sirringhaus, M. Heeney, I. McCulloch, *J. Am. Chem. Soc.*, 2011, **133**, 3272; (c) X. Guo, R. Ortiz, Y. Zheng, M. Kim, S. Zhang, Y. Hu, G. Lu, A. Facchetti, T. Marks, *J. Am. Chem. Soc.*, 2011, **133**, 13685; (d) J. Yuen, J. Fan, J. Seifter, B. Lim, R. Hufschmid, A. Heeger and F Wudl, *J. Am. Chem. Soc.*, 2011, **133**, 20799; (e) T. Lei, J. Dou, Z. Ma, C. Yao, C. Liu, J. Wang and J. Pei, *J. Am. Chem. Soc.*, 2012, **134**, 20025; (f) J. Li, X. Qiao, Y. Xiong, W. Hong, X. Gao and H. Li, *J. Mater. Chem. C*, 2013, **1**, 5128; (g) A. Amacher, H. Luo, Z. Liu, M. Bircher, M. Cascella, J. Hauser, S. Decurtins, Deqing Zhang and S. Liu, *RSC Adv.*, 2014, **4**, 2837; (h) G. Van Pruissen, E. Pidko, M. Wienk and R. Janssen, *J. Mater. Chem. C*, 2014, **2**, 731.

7 (a) J. Lee, A. Han, J. Kim, Y. Kim, J. Oh and C. Yang, *J. Am. Chem. Soc.*, 2012, **134**, 20713; (b) Lee, A. Han, H. Yu, T. Shin, C. Yang and J. Oh, *J. Am. Chem. Soc.*, 2013, **135**, 9540; (c) Z. Chen, M. Lee, R. Ashraf, Y. Gu, S. Albert-Seifried, M. Nielsen, B. Schroeder, T. Anthopoulos, M. Heeney, I. McCulloch and H. Sirringhaus, *Adv. Mater.*, 2012, **24**, 647.

8 (a) L. Tan, Y. Guo, Y. Yang, G. Zhang, D. Zhang, G. Yu, W. Xu and Y. Liu, *Chem. Sci.*, 2012, **3**, 2530; (b) H. Luo, Z. Cai, L. Tan, Y. Guo, G. Yang, Z. Liu, G. Zhang, D. Zhang, W. Xu and Y. Liu, *J. Mater. Chem. C*, 2013, **1**, 2688.

9 L. Zhu, Y. Yi, Y. Li, E. Kim, V. Coropceanu and J. L. Brédas, *J. Am. Chem. Soc.*, 2012, **134**, 2340.

10 (a) E. Meijer, D. Deleeuw, S. Setayesh, E. Veenendaal, B. Huisman, P. Blom, J. Hummelen, U. Scherf and T. Klapwijk, *Nat. Mater.*, 2003, **2**, 678; (b) Y. Hayashi, H. Kanamori, I. Yamada, A. Takasu and S. Takagi, *Appl. Phys. Lett.*, 2005, **86**, 052104; (c) A. Babel, Y. Zhu, K. Cheng, W. Chen and S. Jenekhe, *Adv. Funct. Mater.*, 2007, **17**, 2542; (d) K. Szendrei, D. Jarzab, Z. Chen, A. Facchetti and M. Loi, *J. Mater. Chem.*, 2010, **20**, 1317.

11 (a) J. Zhang, H. Geng, T. Virk, Y. Zhao, J. Tan, C. Di, W. Xu, K. Singh, W. Hu, Z. Shuai, Y. Liu and D. Zhu, *Adv. Mater.*, 2012, **24**, 2603; (b) J. Zhang, J. Tan, Z. Ma, W. Xu, G. Zhao, H. Geng, C. Di, W. Hu, Z. Shuai, K. Singh and D. Zhu, *J. Am. Chem. Soc.*, 2013, **135**, 558; (c) S. Park, S. Varghese, J. Kim, S. Yoon, O. Kwon, B. An, J. Gierschner and S. Park, *J. Am. Chem. Soc.*, 2013, **135**, 4757.

12 (a) Z. Chen, Y. Zheng, H. Yan and A. Facchetti, *J. Am. Chem. Soc.*, 2009, **131**, 8; (b) H. Yan, Z. Chen, Y. Zheng, C. Newman, J. Quinn, F. Dotz, M. Kastler and A. Facchetti, *Nature*, 2009, **457**, 679; (c) X. Zhan, A. Facchetti, S. Barlow, T. Marks, M. Ratner, M. Wasielewski and S. Marder, *Adv. Mater.*, 2011, **23**, 268; (d) D. Hwang, R. Dasari, M. Fenoll, V. Alain-Rizzo, A. Dindar, J. Shim, N. Deb, C. Fuentes-Hernandez, S. Barlow, D. Bucknall, P. Audebert, S. Marder and B. Kippelen, *Adv. Mater.*, 2012, **24**, 4445.

13 (a) X. Gao, C. Di, Y. Hu, X. Yang, H. Fan, F. Zhang, Y. Liu, H. Li and D. Zhu, *J. Am. Chem. Soc.*, 2010, **132**, 3697; (b) Y. Zhao, C. Di, X. Gao, Y. Hu, L. Zhang, Y. Liu, J. Wang, W. Hu and D. Zhu, *Adv. Mater.*, 2011, **23**, 2448; (c) Y. Hu, X. Gao, C. Di, X. Yang, F. Zhang, Y. Liu, H. Li and D. Zhu, *Chem. Mater.*, 2011, **23**, 1204.

14 (a) X. Chen, Y. Guo, L. Tan, G. Yang, Y. Li, G. Zhang, Z. Liu, W. Xu and D. Zhang, *J. Mater. Chem. C*, 2013, **1**, 1087; (b) X. Chen, J. Wang, G. Zhang, Z. Liu, W. Xu and D. Zhang, *New J. Chem.*, 2013, **37**, 1720.

15 (a) L. Polander, S. Tiwari, L. Pandey, B. Seifried, Q. Zhang, S. Barlow, C. Risko, J. Brédas, B. Kippelen and S. Marder, *Chem. Mater.*, 2011, **23**, 3408; (b) S. Suraru, U. Zschieschang, H. Klauk and F. Würthner, *Chem. Commun.*, 2011, **47**, 11504.

16 X. Gao, W, Qiu, X. Yang, Y. Liu, Y. Wang, H. Zhang, T, Qi, Y. Liu, K. Lu, C. Du, Z. Shuai, G. Yu, D. Zhu, *Org. Lett.*, 2007, **9**, 3917.

17 L. Dou, J. Gao, E. Richard, J. You, C. Chen, K. Cha, Y. He, G. Li and Y. Yang. *J. Am. Chem. Soc.*, 2012, **134**, 10071.

18 Apart from increasing the crystallinity for the blending thin film, charge transfer interactions between **4NH$_2$-NDI** and **DHNDI** within the blending thin film, which may lead to lowering the resistance at the metal/organic interface and in the channel region, may also play an important role in improving the performances of OFETs (see, E. Lim, B. Jung, M. Chikamatsu, R. Azumi, Y. Yoshida, K. Yase, L. Do, H. Shim, *J. Mater. Chem.* 2007, **17**, 1416; L. Ma, W. Lee, Y. Park, J. Kim, H. Lee, K. Cho, *Appl. Phys. Lett.* 2008, **92**, 063310.). However, it is still rather difficult to determine the intermolecular arrangements of **4NH$_2$-NDI** and **DHNDI**. Thus, it is hard to know whether the superexchange intermolecular coupling (see ref. 9) exist within the blend thin film.

19 J. Reczek, K. Villazor, V. Lynch, T. Swager and B. Iverson, *J. Am. Chem. Soc.*, 2006, **128**, 7995.

Journal of Materials Chemistry C Accepted Manuscript